THE JOURNAL OF BIOLOGICAL CHEMISTRY VOL. 285, NO. 2, pp. 1435–1445, January 8, 2010

Structure of the N-terminal Regulatory Domain of a Plant NADPH Oxidase and Its Functional Implications*[S]

Received for publication, August 24, 2009, and in revised form, October 8, 2009 Published, JBC Papers in Press, October 28, 2009, DOI 10.1074/jbc.M109.058909

Takashi Oda[‡], Hiroshi Hashimoto[‡], Naoyuki Kuwabara[‡], Satoko Akashi[‡], Kokoro Hayashi[§], Chojiro Kojima[§], Hann Ling Wong[¶], Tsutomu Kawasaki[¶], Ko Shimamoto[¶], Mamoru Sato[‡], and Toshiyuki Shimizu[‡1]

From the [‡]Graduate School of Nanobioscience, Yokohama City University, 1-7-29 Suehiro-cho, Tsurumi-ku, Yokohama, Kanagawa 230-0045 and the Laboratories of [§]Biophysics and [¶]Plant Molecular Genetics, Nara Institute of Science and Technology, 8916-5 Takayama, Ikoma, Nara 630-0192, Japan

Plant NADPH oxidases (Rboh, for respiratory burst oxidase homolog) produce reactive oxygen species that are key regulators of various cellular events including plant innate immunity. Rbohs possess a highly conserved cytoplasmic N-terminal region containing two EF-hand motifs that regulate Rboh activity. Rice (*Oryza sativa*) RbohB (OsRbohB) is regulated by the direct binding of a small GTPase (Rac1) to this regulatory region as well as by Ca^{2+} binding to the EF-hands. Here, we present the atomic structure of the N-terminal region of OsRbohB. The structure reveals that OsRbohB forms a unique dimer stabilized by swapping the EF-hand motifs. We identified two additional EF-hand-like motifs that were not predicted from sequence data so far. These EF-hand-like motifs together with the swapped EF-hands form a structure similar to that found in calcineurin B. We observed conformational changes mediated by Ca^{2+} binding to only one EF-hand. Structure-based *in vitro* pulldown assays and NMR titration experiments defined the OsRac1 binding interface within the coiled-coil region created by swapping the EF-hands. In addition, we demonstrate a direct intramolecular interaction between the N and C terminus, and that the complete N-terminal cytoplasmic region is required for this interaction. The structural features and intramolecular interactions characterized here might be common elements shared by Rbohs that contribute to the regulation of reactive oxygen species production.

The rapid generation of reactive oxygen species (ROS)[2] such as superoxide (O_2^-) and hydrogen peroxide (H_2O_2) is considered to be a component of the resistance response of plants to pathogens. ROS play multiple roles as signals that mediate responses to biotic and abiotic stresses, developmental cues, and programmed cell death. ROS accumulation during early stages of plant defense reponse is known as the oxidative burst (1). The oxidative burst can further trigger the collapse of challenged host cells at the onset of the hypersensitive response and generate signals for defense gene induction. ROS are generated by plant NADPH oxidases and genes termed *rboh* (respiratory burst oxidase homolog) that encode homologs of the mammalian NADPH oxidase catalytic subunit $gp91^{phox}$, have been isolated from many plant species including rice, *Arabidopsis*, tobacco, and potato (2–7).

The phagocyte enzymatic complex of NADPH oxidase (known as flavocytochrome b_{558}) consists of two membrane proteins, $gp91^{phox}$ (Nox2) and $p22^{phox}$. Upon cell activation in mammals, the three cytosolic regulatory proteins, $p47^{phox}$, $p67^{phox}$, and $p40^{phox}$, and the small GTPase Rac translocate from the cytosol, assemble, and activate flavocytochrome b_{558} at the cell membrane. However, the mammalian cytosolic regulatory proteins ($p47^{phox}$, $p67^{phox}$, and $p40^{phox}$) and $p22^{phox}$ are missing in plants (8). Furthermore, unlike the mammalian $gp91^{phox}$, all plant Rboh proteins carry a cytosolic N-terminal region with two EF-hands that bind Ca^{2+} (Fig. 1*A*) (3, 8). Although these motifs are absent from the mammalian $gp91^{phox}$, they are present in non-phagocytic NADPH oxidases such as Nox5, Duox1, and Duox2 (9, 10).

Rboh is stimulated directly by Ca^{2+}, likely through the N-terminal region (11). Recently, it has been reported that Ca^{2+} activated the *Arabidopsis* NADPH oxidase, RHD2 (AtRbohC), to produce ROS at the growing tip of root hairs. Moreover, Ca^{2+} binding to EF-hand motifs is required for activation of ROS production by RHD2 (12). Recent work has also demonstrated that calcium-dependent protein kinases activate potato RbohB (StRbohB) protein by phosphorylation of the N-terminal region (13), and that Ca^{2+} binding and phosphorylation synergistically activate ROS production by AtRbohD (14). These results demonstrate that the extended N-terminal region plays a key role in the regulation of Rboh.

OsRac1, a Rac GTPase located in the plasma membrane, functions as a positive regulator of NADPH oxidase activity and is involved in defense responses in rice (15, 16). In fact, constitutively active and dominant-negative forms of OsRac1 were found to activate and suppress ROS production, respectively. Direct interaction between the constitutively active OsRac1 and the N-terminal region of OsRbohB was verified by yeast two-hybrid analysis, *in vitro* pulldown assays, NMR titration experiments, and *in vivo* fluorescence resonance energy trans-

* This work was supported in part by the Targeted Proteins Research Program (TPRP) and grants-in-aid for scientific research from the Ministry of Education, Culture, Sports, Science and Technology (MEXT), Japan.

[S] The on-line version of this article (available at http://www.jbc.org) contains supplemental Figs. S1–S3 and Table S1.

The atomic coordinates and structure factors (code 3A8R) have been deposited in the Protein Data Bank, Research Collaboratory for Structural Bioinformatics, Rutgers University, New Brunswick, NJ (http://www.rcsb.org/).

[1] To whom correspondence should be addressed. Tel.: 81-45-508-7226; Fax: 81-45-508-7365; E-mail: shimizu@tsurumi.yokohama-cu.ac.jp.

[2] The abbreviations used are: ROS, reactive oxygen species; GST, glutathione *S*-transferase; GMP-P(NH)P, guanyl-5′-yl imidodiphosphate; Bis-Tris, 2-[bis(2-hydroxyethyl)amino]-2-(hydroxymethyl)propane-1,3-diol; ESI-MS, electrospray ionization-mass spectrometry; SAXS, small angle x-ray scattering.

fer microscopy (17). OsRac1 has also been shown to activate cinnamoyl-CoA reductase, a key enzyme in lignin biosynthesis, thus regulating the biosynthesis of lignin precursors (monolignols) that can be polymerized by H_2O_2-consuming peroxidases in the cell wall (18). These studies indicated that Rac GTPases interact coordinately with downstream pathways through regulation of multiple effector proteins. The elucidation of the regulatory mechanisms should be of great interest in plant signal transduction research.

Here we present the first crystal structure of the N-terminal region of OsRbohB, revealing that two molecules form a dimer with swapped EF-hands and that OsRbohB contains two additional EF-hand-like motifs so far not predicted from sequence analysis. We show that Ca^{2+} binding to the EF-hands is necessary for the Ca^{2+}-mediated conformational change. Structure-based mutagenesis and NMR studies revealed that key residues for the interaction of OsRbohB and OsRac1 are located in the coiled-coil region created by EF-hand swapping. Here we demonstrate for the first time a direct intramolecular interaction between the N terminus and C terminus for which the complete N-terminal cytoplasmic region is required. The highly conserved amino acid sequences of the N- and C-terminal regions suggest that the structural features and intramolecular interactions characterized here might be common elements shared by Rbohs that contribute to the regulation of ROS production.

EXPERIMENTAL PROCEDURES

Expression and Purification—Details on the expression, purification, and crystallization of OsRbohB-(138–313) have been published (19). In brief, OsRbohB-(138–313) was expressed in *Escherichia coli* and the protein product was purified using DEAE-Sepharose fast flow (GE Healthcare), nickel-nitrilotriacetic acid-agarose (Qiagen), HiTrapQ HP (GE Healthcare), and Superdex75 (GE Healthcare). 2 mM $CaCl_2$ was added throughout the purification. Purified protein was concentrated to 10–40 mg/ml. All site-directed mutant proteins were prepared using the QuikChange kit (Stratagene).

Crystallization and X-ray Data Collection—OsRbohB-(138–313) was crystallized using polyethylene glycol 8,000 as a precipitant containing $CaCl_2$ (19). Crystals of SeMet-labeled OsRbohB-(138–313) were obtained using 0.1 M HEPES pH 7.0 buffer containing 15% (w/v) polyethylene glycol 8,000, (0048) 1.0 M NaSCN, and 10 mM dithiothreitol. Protein concentration was 16 mg/ml. X-ray diffraction data were collected at −173 °C on beamline BL41XU at SPring-8 (Harima, Japan) and beamline NW-12 at Advanced Ring (PF-AR), Tsukuba, Japan. Before the x-ray experiments, crystals of OsRbohB-(138–313) and SeMet-labeled OsRbohB-(138–313) were soaked in crystallization buffer containing 20% ethylene glycol as a cryoprotectant. Diffraction data were processed with HKL2000 (20). The crystallographic data and data collection statistics of OsRbohB-(138–313) and SeMet-labeled OsRbohB-(138–313) are provided in Table 1.

Structure Determination and Refinement—The structure of OsRbohB-(138–313) was solved by multiwavelength anomalous diffraction using the SeMet-labeled OsRbohB-(138–313) crystal. Experimental phases were calculated up to 3.0-Å resolution with SOLVE (21) and improved by solvent-flattening with RESOLVE (22). An initial model was built by ARP/wARP (23), followed by COOT (24), and refined with CNS (25). The model was refined using REFMAC (26) with no NCS restraints and then cycled with rebuilding in COOT. TLS refinement was incorporated into the later stages of the refinement process with each chain as a separate TLS group. The model finally converged, resulting in a crystallographic *R* value of 23.4% and a free *R* value of 26.6% for all diffraction data up to 2.4-Å resolution. The final model quality was assessed using PROCHECK (27) and MolProbity (45). The Ramachandran plot of the final model, containing 333 amino acid residues, 2 calcium ions, and 77 water molecules, shows that all amino acid residues were in the most favored and allowed region as defined by PROCHECK. The final refinement statistics are summarized in Table 1 and the output of Molprobity is shown in supplemental Table S1. The figures were generated by PyMOL (28). The surface area was calculated by PROTORP (29). Coordinates for OsRbohB-(138–313) are being deposited in the Protein Data Bank of the Research Collaboratory for Structural Bioinformatics (Protein Data Bank code 3A8R).

In Vitro Pulldown Assay—GST-OsRac1 was expressed in *E. coli* strain BL21 star (DE3) and purified using glutathione-Sepharose resin and Superdex200 (GE Healthcare). Purified GST-OsRac1 was incubated with 4 mM GDP or GMP-P(NH)P (Sigma) in 20 mM BisTris, pH 6.8, 5 mM EDTA, and 1 mM dithiothreitol. Nucleotide exchange was stopped by addition of 20 mM $MgCl_2$. This reaction was repeated twice. After absorbing the GST-tagged proteins onto 15–30 μl of glutathione-Sepharose 4B resin, 30–40 μl of the solution containing 0.8 mM purified OsRbohB-(138–313) were applied and incubated at 4 °C for 12 h. After the beads were washed with a buffer solution (50 mM BisTris, pH 6.8, 50 mM KCl, 5 mM $MgCl_2$, 2 mM $CaCl_2$, 1 mM phenylmethylsulfonyl fluoride, 3%, v/v, dimethyl sulfoxide), bound proteins were analyzed by SDS-PAGE.

TABLE 1
Data collection and refinement statistics

	SeleniumMet-labeled			Native
	Peak	Edge	Remote	
X-ray source		PFBL5A		SPring8 BL41XU
Wavelength (Å)	0.97915	0.97931	0.96411	1.00000
Space group	$P2_12_12_1$	$P2_12_12_1$	$P2_12_12_1$	$P2_12_12_1$
a (Å)	61.1	61.1	61.2	60.4
b (Å)	77.7	77.7	77.8	72.2
c (Å)	111.9	112.0	112.1	118.9
Resolution (Å)	50.0-3.0	50.0-3.0	50.0-3.0	50.0-2.4
No. observations	72,749	72,617	69,369	137,001
No. uniques	10,948	10,965	10,976	20,590
R_{merge} (%)[a,b]	8.8 (22.4)	6.7 (19.3)	6.3 (19.1)	4.8 (23.4)
Completeness (%)[a]	97.7 (82.1)	96.6 (75.3)	96.5 (75.1)	97.7 (86.0)
$I/\sigma(I)$[a]	14.7 (4.9)	13.0 (3.8)	13.2 (4.0)	16.3 (6.0)
R_{work}/R_{free} (%)[c]				23.4/26.6
R.M.S. deviation				
Bond length (Å)				0.016
Bond angle (°)				1.500
Ramachandran plot				
Most favored (%)				91.1
Additional allowed (%)				8.5
Disallowed (%)				0
No. nonhydrogen atom				2,698

[a] Values in parentheses are for the highest resolution shell. The resolution ranges of the outer shells are 3.24–3.0 Å for native data and 2.49–2.40 Å for selenium derivative data.
[b] $R_{merge} = \Sigma|I - \langle I\rangle|/\Sigma I$; calculated for all data.
[c] R_{work} and $R_{free} = \Sigma\|F_o| - |F_c\|/\Sigma|F_o|$, where the free reflections (5% of the total used) were held aside for R_{free} throughout refinement.

cDNAs of four N-terminal regions of OsRbohB fused to Trx (OsRbohB-(1–355), OsRbohB-(1–306), OsRbohB-(1–137), and OsRbohB-(138–313)) were subcloned into the pCOLA Duet1 vector. The C-terminal region of OsRbohB consisting of the residues from position 590 to the C terminus and the cytosolic loop region were subcloned into pMAL c2E vectors. These two proteins were coexpressed in *E. coli* strain BL21(DE3) Codon Plus RIL. Cells were suspended in lysis buffer (50 mM HEPES-NaOH, pH 7.5 containing 50 mM KCl, 10% (v/v) glycerol, 7 mM 2-mercaptoethanol, 0.05% (v/v) Tween 20, 10 mM imidazole, pH 7.5, and 2 mM $CaCl_2$ or 2 mM EDTA) and then disrupted by sonication on ice. The supernatant was absorbed onto 30 μl of amylose resin and the bound proteins were eluted with 40 μl of lysis buffer containing 20 mM maltose. Eluted proteins were analyzed by SDS-PAGE and subjected to Western blot with anti-His (GE Healthcare).

CD Measurements—CD spectra were acquired at room temperature (25 °C) using a Jasco J-720W, which was set for a 200–250-nm wavelength range. Samples of 190 μM Ca^{2+}-bound or Ca^{2+}-free forms of OsRbohB-(138–313) dissolved in buffer A (50 mM KCl, 5 mM HEPES-NaOH (pH 7.5), 1 mM dithiothreitol, plus 2 mM $CaCl_2$ or 2 mM EDTA-NaOH) were analyzed.

ESI-Mass Spectrometry (ESI-MS)—ESI mass spectra were acquired using a Q-Tof2 (Waters) with a nano-ESI ion source. Mass spectra from m/z 2000 to 6000 or 8000 were obtained by calibration with (CsI)nCs+. MassLynx version 3.5 software (Waters) was used for data processing and peak integration. The parameters for ESI-mass spectrometry were similar to those previously reported (45). The temperature of the ion source was set to 80 °C. An aliquot of 4 μl of sample solution was deposited in a nanospray glass tip (Waters) and introduced into a nano-ESI source. To observe protein complexes, the pressure in the quadrupole ion guide of the Q-Tof2 was maintained at 8×10^{-3} pascals by throttling down the speedivalve fitted to the rotary pump for the ion source region.

Small Angle X-ray Scattering (SAXS)—SAXS measurements were carried out at the RIKEN structural biology beam-line I (BL45XU) at SPring-8 (Hyogo, Japan). SAXS data were collected at 20 °C on an imaging plate using Rigaku R-AXIS IV^{++}. The sample to detector distance was determined to be 2004 mm by silver behenate as a standard sample in the SAXS experiment. Three successive measurements were made for each solution with an exposure time of 100 s and wavelength of 1.0000 Å, and a circular average was made to obtain one-dimensional intensity data. The SAXS profiles of Ca^{2+}-bound and Ca^{2+}-free forms of OsRbohB-(138–313) (0.9 mM) containing buffer A was compared. To detect structural changes induced by Ca^{2+} binding, the middle- and high-angle ranges of the scattering curves, which contain information on secondary structures, were compared.

NMR Titration—All NMR experiments were recorded on a Bruker Avance 500 NMR spectrometer at 30 °C using 0.15 mM ^{15}N OsRac1 in 50 mM BisTris, pH 6.8, 50 mM KCl, 5 mM $MgCl_2$, 1 mM dithiothreitol, and 10% D_2O. The binding of OsRac1 to OsRbohB-(138–313) was monitored by ^{1}H-^{15}N heteronuclear single quantrum coherence experiments, titrating non-labeled OsRbohB-(138–313) in a concentration range from 15 to 600 μM.

RESULTS

Overall Structure—The N-terminal region of OsRbohB containing residues 138–313 (hereafter referred to as OsRbohB-(138–313)) has a structure composed of 8 α-helices (αA–αH) and 2 short β-strands (β1, β2). The amino acid sequence of the molecule, together with assignments of the secondary structure elements, is shown in Fig. 1*B*. Two molecules (molecules A and B) are present in the asymmetric crystal unit (Fig. 1*C*). Residues 304–313 in molecule A and residues 305–313 in molecule B were disordered. Surprisingly, the C-terminal region (residues 263–303) of one molecule is swapped into the core domain (residues 138–262) of the other molecule. As described below, the EF-hand of one molecule is packed together with the corresponding EF-hand of the other molecule (Fig. 2*B*, *left*). An intermolecular coiled-coil structure (residues 251–285) connects the two molecules (Fig. 1*C*). With the exception of the swapped region, the core domains were superposed well with root mean square deviations of 0.81 Å for Cα atoms, whereas the superposition of the whole structures yielded root mean square deviations of 3.0 Å for Cα atoms, indicating that orientation of the C-terminal region is different between the two molecules.

In the swapped dimer, there are two kinds of interfaces, one being the region between the swapped EF-hands and the other being a coiled-coil region formed by the swapping. The contact area of the swapped EF-hands is ~1133 $Å^2$, and contains hydrophobic contacts as well as a few hydrogen bonds. The region that forms the coiled-coil structure (residues 260–274) exhibits a loose packing with a contact area of 268 $Å^2$, suggesting that the dimer is mainly stabilized by the swapped EF-hands and that the coiled-coil structure contributes to stabilization merely to a minor extent.

The assembled protomer structure composed of the core domain and the swapped C-terminal region has a three-dimensional structure similar to calcineurin B and recoverin (Fig. 2*C*), which contain four EF-hands in a highly compact, globular structure, in contrast to the dumbbell arrangement of calmodulin. In fact, a structural similarity search using DALI (30) revealed that the protomer structure of OsRbohB-(138–313) shares structural similarity with calcineurin B (PDB accession code 1AUI) with a Z-score of 11.1 and a sequence identity of 16% (135 equivalent residues). It also revealed similarity with recoverin (PDB accession code 2d8n) with a Z-score of 8.4 and 14% sequence identity.

EF-hand-containing proteins such as calcineurin B and recoverin have a hydrophobic pocket on the side of the molecule opposite the EF-hands. In these proteins, the conformation of the C-terminal α-helix varies and affects the degree to which the hydrophobic pocket is exposed. OsRbohB-(138–313) also possesses a hydrophobic pocket. Interestingly, the N-terminal amino acids 139–156 of OsRbohB-(138–313) adopt a helical conformation and are located in the hydrophobic pocket (Fig. 2*C*). The hydrophobic residues (Ala^{142}, Val^{144}, Ala^{145}, Leu^{146}, Leu^{149}, Phe^{151}, Val^{152}, and Val^{156}) in the N-terminal helix are in close contact with the hydrophobic pocket. The opposite face of the N-terminal helix has a hydrophilic nature with polar and charged residues that point toward the solvent.

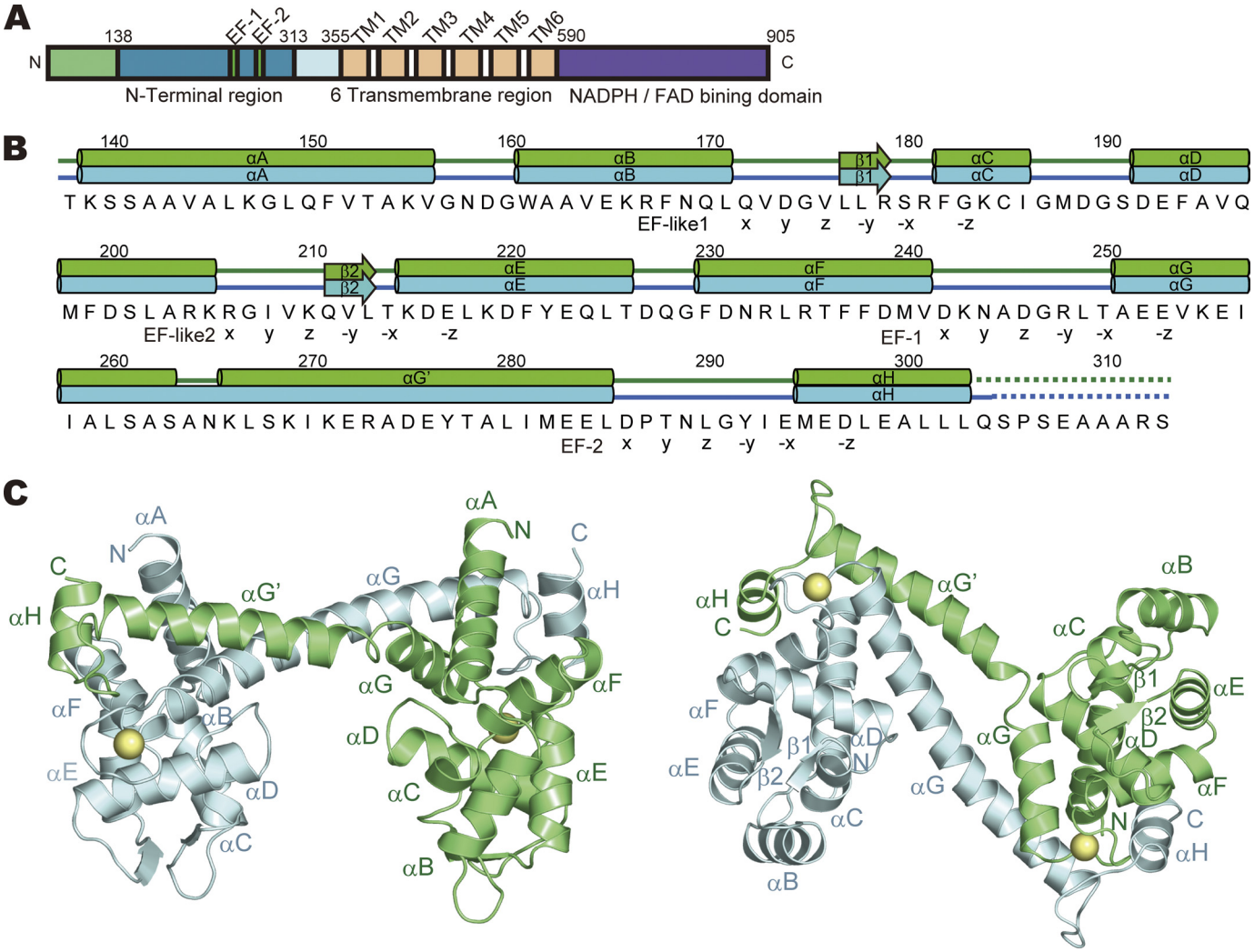

FIGURE 1. **Structure of OsRbohB-(138–313).** *A*, domain structure of OsRbohB. *B*, sequence of OsRbohB-(138–313). Secondary structure elements are shown on *top*, with tubes representing α-helices (αA–αH) and *arrows* the β-strands (β1, β2). *Dotted lines* highlight disordered regions. EF-hands and EF-hand-like motifs are marked *below* the sequence (X, Y, Z, -Y, -X, and -Z) according to the typical EF-hand motif. *C*, ribbon models of OsRbohB-(138–313) viewed from the side (*left*) and bottom (*right*). Two molecules (molecule A, *green*; molecule B, *cyan*) are paired by domain swapping. Ca^{2+} ions are shown as *yellow spheres*.

Number of Ca^{2+} Ions in the Protein—One peak appeared on the difference Fourier map with a contour level higher than 5 σ in EF-1 (Fig. 2*A*), although the OsRbohB amino acid sequence suggests the presence of two EF-hand motifs (Fig. 1A, *EF-1* and *EF-2*). This single peak was scrutinized using an anomalous Fourier map calculated with FFT program in the CCP4 suite (31) based on the diffraction data collected at λ = 1.6000 Å. The anomalous Fourier map showed a significant peak with contour levels above 7 σ corresponding to the single peak. We also confirmed the number of calcium ions coordinated in OsRbohB by ESI-MS. Fig. 3*A* shows ESI mass spectra of 50 μM of the wild type and E253A mutant of OsRbohB-(138–313) in the presence of 5.7 μM Ca^{2+}. The peak at *m*/*z* 2006.56 in Fig. 3*A* corresponds to $[M + 9H]^{9+}$ of OsRbohB-(138–313). Two satellite peaks at *m*/*z* 2009.11 and 2210.97 correspond to $[M + 8H + Na]^{9+}$ and $[M + 7H + Ca]^{9+}$, respectively. By deconvolution of the acquired spectrum, the observed molecular mass of OsRbohB-(138–313) alone was estimated to be 19,851.5; the mass with one calcium ion bound was 19,888.1, in good agreement with the expected values (19,850.6 and 19,888.7). Following addition of EDTA, the Ca^{2+}-bound species disappeared from the ESI mass spectrum (data not shown). This is consistent with the fact that only one peak was observed in the electron density map. Therefore, the protein binds one calcium mole per mol of protein. In contrast, the E253A mutant, in which Ca^{2+} binding is expected to be disturbed because of the substitution of Glu, which is important for Ca^{2+} coordination in the first EF-hand motif, gave protonated molecules of only one species in the ESI mass spectrum (Fig. 3*A*). The observed molecular mass of the E253A mutant was 19,793.6, well in line with the theoretical value of 19,792.6, corroborating that the E253A mutant does not bind Ca^{2+}.

Two Predicted EF-hands Motifs and Two Unpredicted EF-hand Motifs—The canonical Ca^{2+}-binding EF-hand (EF-1) forms a conventional helix-loop-helix EF motif (αF–αG) and the calcium ion is coordinated in the typical pentagonal-bipyramidal geometry (Fig. 2*A*, *EF-1*). In EF-1 of OsRbohB, the side chains of Asp^{242}, Asn^{244}, Asp^{246}, and Glu^{253} coordinate a Ca^{2+} ion with Glu^{253} as a bidentate substrate. Arg^{248} ligates the Ca^{2+} ion through its carbonyl oxygen and also coordinates a water

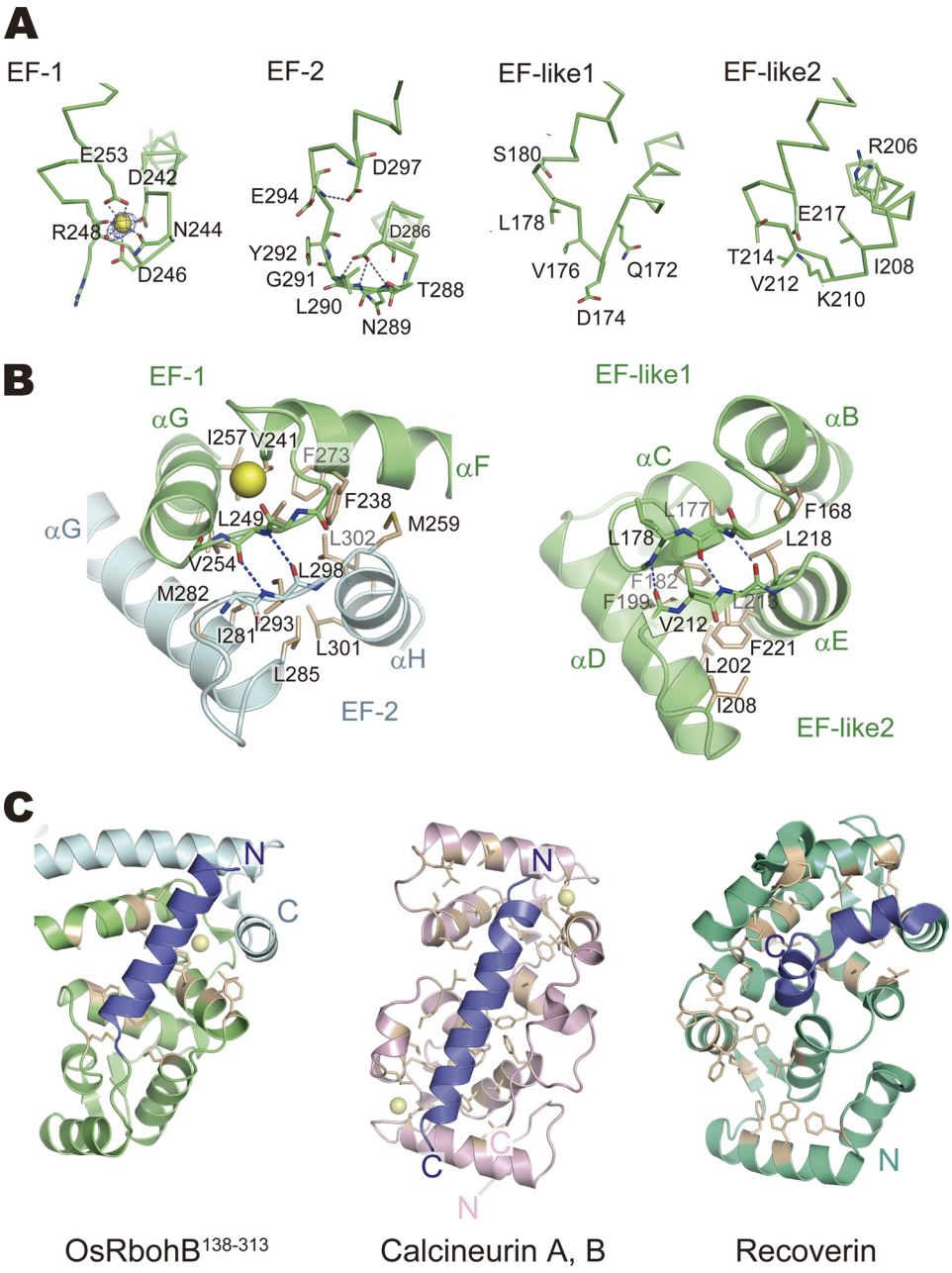

FIGURE 2. **EF-hand motifs of OsRbohB-(138–313) and similar proteins.** *A*, representation of EF-hand motifs (EF-1, EF-2, EF-like 1, and EF-like 2). Difference Fourier maps showing contour levels higher than 5 σ. Ca^{2+} ion and water molecules are represented as a *yellow* and *red spheres*, respectively. Amino acid residues of EF-hand motifs at positions X to Z are shown as *sticks*. *B*, magnified view of EF-hand pairs composed of EF-1 and EF-2, and EF-like 1 and EF-like 2, respectively. Residues forming the hydrophobic cores are shown as *white sticks*. *C*, hydrophobic pockets of OsRbohB-(138–313), calcineurin B, and recoverin. Residues forming the hydrophobic pocket are shown as *white sticks*. The pocket of OsRbohB-(138–313) formed by swapped EF-hands and EF-hand-like motifs is occupied by an N-terminal helix (*blue*) protruding from the core domain. The pockets of calcineurin B and recoverin are occupied by α-helices protruding from calcineurin A and the C-terminal region (*blue*), respectively.

molecule that ligates Ca^{2+}. In contrast, the sequence of EF-2 (αG–αH) significantly deviates from the canonical one and no bound Ca^{2+} was identified. The structure of EF-2 is stabilized through internal interactions. Asp^{286} interacts with main chain atoms of Asn^{289}, Leu^{290}, and Gly^{291}, and the main chain atom of Glu^{294} is hydrogen-bonded to Asp^{297} (Fig. 2*A*, *EF-2*).

Generally, proteins containing EF-hand motifs have a domain formed by a pair of EF-hands. It should be noted that the EF-1 motif of one OsRbohB molecule makes extensive hydrophobic and hydrogen-bond contact with the EF-2 motif of its partner, thereby forming a domain in a similar way as conventional EF-hand pairs (Fig. 2*B*, *left*).

Sequence analysis suggested no EF-hands other than EF-1 and EF-2, but the structure definitely shows two additional EF-hands, EF-like 1 (αB–αC) and EF-like 2 (αD–αE; Fig. 2*A*). In general, the structural integrity of the EF-hand domain is maintained by the backbone hydrogen bonds in a short anti-parallel β-sheet, and by numerous hydrophobic contacts between the helices. The domain formed by EF-like 1 and EF-like 2 preserved this structural feature of the EF-hand, although the sequences of EF-like 1 and 2 are completely different from the canonical EF-hand motif. In fact, Phe^{168}, Leu^{177}, and Phe^{182} of EF-like 1 are in close proximity to Ile^{208}, Leu^{213}, Leu^{218}, and Phe^{221} of EF-like 2 and form a hydrophobic core. Leu^{177} of EF-like 1 and Leu^{213} of EF-like 2 interact through backbone hydrogen bonds in such a way that they form an anti-parallel β-sheet (Fig. 2*B*, *right*).

Ca^{2+}-mediated Conformational Change—We measured far-UV CD to examine the effect of Ca^{2+} binding. Consistent with the three-dimensional structure, the CD spectrum of OsRbohB-(138–313) showed two negative minimum at around 208 and 222 nm, which is typical of α-helical proteins. The CD spectra differed between the Ca^{2+}-bound and Ca^{2+}-free forms (Fig. 3*C*, *left*). In contrast, the E253A mutant underwent no obvious conformational change following addition of Ca^{2+} (Fig. 3*C*, *right*). This result suggests that OsRbohB changes its conformation in a calcium-dependent manner and may function as a molecular switch.

To gain further insight into the behavior of the protein in solution, we measured SAXS profiles of the wild type and E253A mutant of OsRbohB-(138–313). The SAXS profile of OsRbohB-(138–313) was modified by Ca^{2+} in the q range from 0.2 to 0.35 $Å^{-1}$ (Fig. 3*D*, *left*), whereas no such effect was observed in the E253A mutant (Fig. 3*D*, *right*).

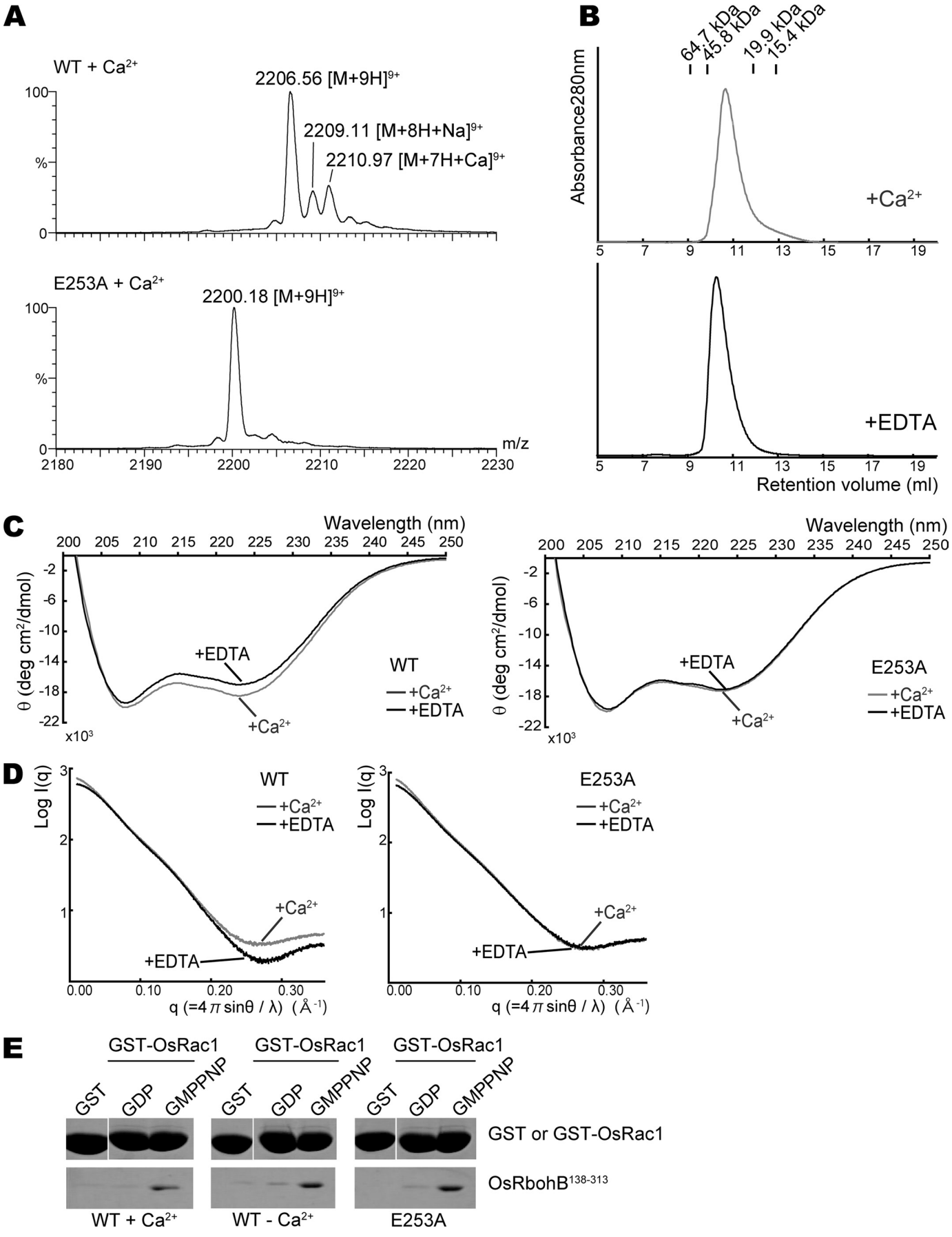
A
WT + Ca2+
2206.56 [M+9H]9+
2209.11 [M+8H+Na]9+
2210.97 [M+7H+Ca]9+
100
%
0
E253A + Ca2+
2200.18 [M+9H]9+
m/z
2180
2190
2200
2210
2220
2230
B
64.7 kDa
45.8 kDa
19.9 kDa
15.4 kDa
Absorbance280nm
+Ca2+
+EDTA
5
7
9
11
13
15
17
19
Retention volume (ml)
C
Wavelength (nm)
200
205
210
215
220
225
230
235
240
245
250
θ (deg cm2/dmol)
-2
-6
-10
-14
-18
-22
x10³
+EDTA
+Ca2+
WT
+Ca2+
+EDTA
E253A
D
Log I(q)
3
2
1
WT
+Ca2+
+EDTA
E253A
0.00
0.10
0.20
0.30
q (=4π sinθ / λ) (Å-1)
E
GST-OsRac1
GST
GDP
GMPPNP
GST or GST-OsRac1
OsRbohB138-313
WT + Ca2+
WT - Ca2+
E253A

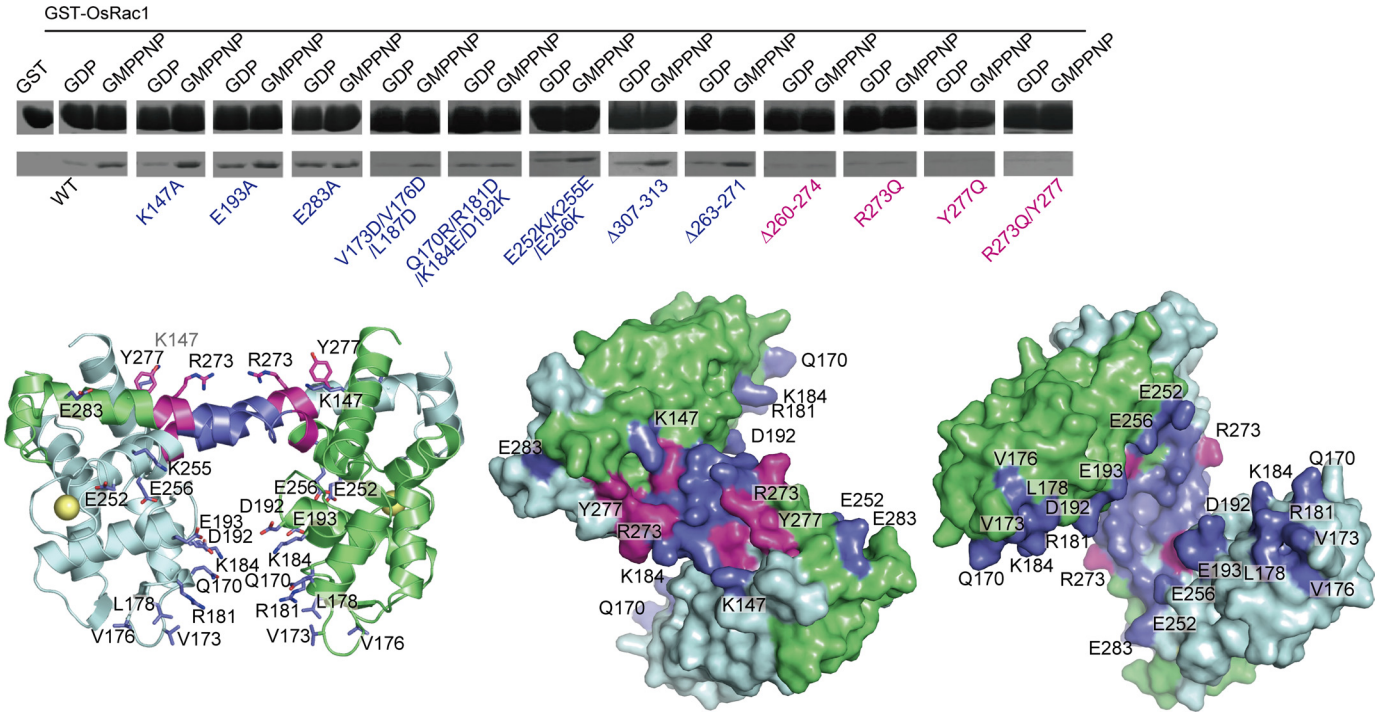

FIGURE 4. **Interaction between OsRbohB-(138–313) and OsRac1.** *In vitro* pulldown assays using OsRbohB-(138–313) mutants and GST-OsRac1. Mutation and deletion sites are mapped onto the structure of OsRbohB-(138–313) shown as a ribbon model and as surface representations (two views from opposite sides). Residues that are necessary to maintain the full binding affinity are colored *magenta*, whereas residues exhibiting no or little effect on the binding are shown in *blue*.

We performed *in vitro* pulldown assays using the wild type and E253A mutant of OsRbohB-(138–313) to investigate the Ca^{2+} dependence of the binding to OsRac1. Both proteins preferentially bound to OsRac1 in the GTP-bound form with a similar affinity, indicating that OsRac1 binding is not affected by Ca^{2+} (Fig. 3*E*).

Interaction with OsRac1—We performed *in vitro* pulldown assays using OsRbohB-(138–313) mutants to identify residues mediating the interaction of OsRbohB with OsRac1 (Fig. 4*A*). K147A in the N-terminal helix, E193A in αD, and E283A in EF-2 did not affect the binding affinity. The triple (V173D/V176D/L178D) and quadruplex (Q170R/R181D/K184E/D192K) mutations near the EF-like 1 motif maintained the binding affinity, and so did the triple (E252K/K255E/E256K) mutation in EF-1. These results suggested that the core domain of OsRbohB-(138–313) is not part of the binding interface for OsRac1 (Fig. 4*A*). Similarly, the affinity did not change following truncation of 7 residues (Δ307–313) in the C terminus where the protein structure was disordered.

The deletion of 9 residues (Δ263–271) in the central coiled-coil region had little effect on interaction with OsRac1, but a 15-residue deletion (Δ260–274) completely abolished OsRac1 binding, suggesting that the flanking region of the central coiled-coil region is essential for binding. Next, we mutated single residues in the flanking region. The single mutation of Arg^{273} to Gln diminished the binding affinity. The Y277Q mutation and double mutations of Arg^{273} and Tyr^{277} markedly reduced the binding affinity. We concluded that the flat surface of the flanking region of the coiled-coil structure served as an OsRac1 binding interface.

To confirm the interaction of OsRac1 with the OsRbohB-(138–313) proteins, an NMR titration experiment was performed. The ^{1}H-^{15}N heteronuclear single quantrum coherence spectrum of the ^{15}N-labeled OsRac1 showed significant signal broadenings induced by direct interaction with OsRbohB-(138–313) (17) (supplemental Fig. S1, *left*). In contrast, little change was observed in the presence of the R273Q/Y277Q mutant of OsRbohB-(138–313) (supplemental Fig. S1, *right*), suggesting weakened interactions with OsRac1.

Ca^{2+}-independent Dimerization Necessary for Rac Binding—We then checked whether Ca^{2+} binding affects the oligomeric state of OsRbohB. The purified protein was eluted from a gel-filtration column at a position corresponding to the homodimer (molecular mass ~39.3 kDa) both in the Ca^{2+}-bound and the Ca^{2+}-free forms (Fig. 3*B*), which were produced by treating the Ca^{2+}-bound form with EDTA. The E253A

FIGURE 3. **Effects of Ca^{2+} binding on dimer formation and the conformation of OsRbohB-(138–313).** *A*, expanded ESI mass spectra of wild-type OsRbohB-(138–313) and the E253A mutant. Stock solutions of both proteins were dialyzed against 500 mM ammonium acetate with 0.2 mM $Ca(CH_3COO)_2$; then, the dialyzed samples were diluted with 500 mM ammonium acetate to prepare solutions of 50 μM protein with 5.7 μM Ca^{2+}. *B*, gel filtration chromatography profiles for Ca^{2+}-bound and EDTA-treated OsRbohB-(138–313). Both are eluted at a similar position. *C*, CD spectra of the wild type (*left*) and E253A mutant (*right*) of OsRbohB-(138–313). *Curves in gray* and *black* show spectra determined in the presence of Ca^{2+} and EDTA, respectively. *D*, scattering curves of SAX in the wild type (*left*) and E253A mutant (*right*) of OsRbohB-(138–313). *Curves in gray* and *black* were determined in the presence of Ca^{2+} and EDTA, respectively. *E*, *in vitro* pulldown assays of GST-OsRac1 with the wild type or E253A mutant of OsRbohB-(138–313). OsRbohB-(138–313) was incubated with GST alone, or with the GDP-bound or the GMP-P(NH)P-bound forms of GST-OsRac1, in the presence or absence of Ca^{2+} (*left* and *middle*). The E253A mutant of OsRbohB-(138–313) was incubated with Ca^{2+} (*right*).

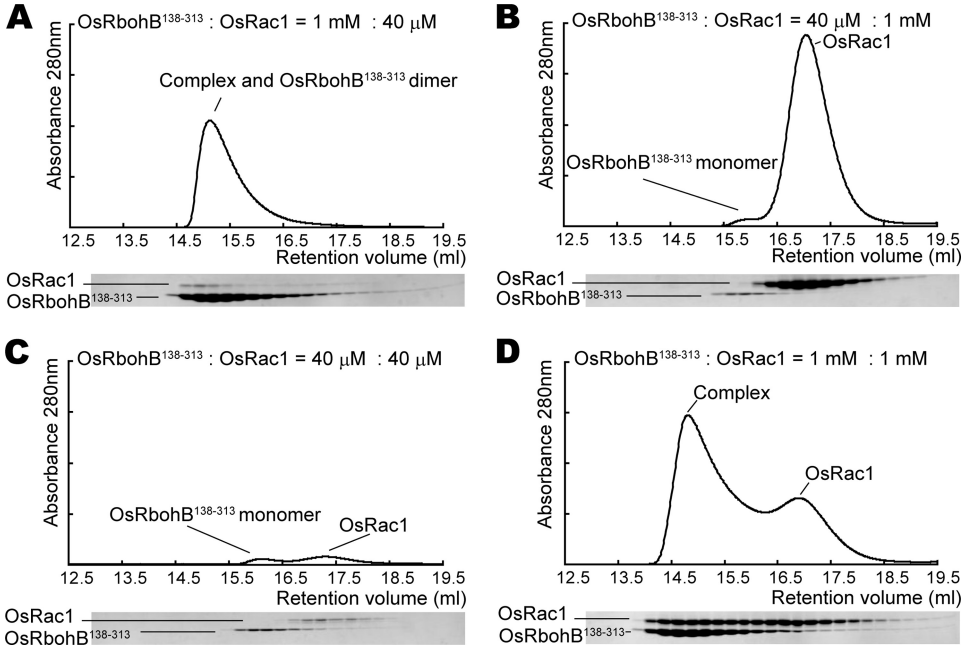

FIGURE 5. **Gel filtration chromatography profiles for mixtures of OsRbohB-(138–313) and OsRac1.** Fractions were analyzed by SDS-PAGE. Peaks corresponding to input proteins and the complex are labeled. *A*, a complex fraction can be detected in a 1 mM:40 μM mixture of OsRbohB-(138–313) and OsRac1. *B* and *C*, no complex fraction is present in 40 μM:1 mM and 40 μM:40 μM mixtures. *D*, a complex fraction and a residual peak for OsRac1 are detectable in a 1:1 mM mixture.

mutant lacking Ca^{2+} binding affinity was also eluted from the same position. In addition, we measured SAXS profiles of the wild type and E253A mutant. In the presence of Ca^{2+}, the molar masses of wild type and E253A mutant proteins were estimated to be 41 and 45 kDa, respectively, corresponding to dimers. The *ab initio* shape analysis of protein in solution by SAXS must be done using the SAXS data at infinite dilution to avoid an interparticle interference effect. Such SAXS data are obtained from SAXS measurements at various protein concentrations. OsRbohB is, however, in equilibrium of dimer-monomer in solution at low protein concentrations, thus indicating that OsRbohB is unsuitable for *ab initio* shape analysis by SAXS. The shape analysis was therefore not carried out in the present study. Self-association was also confirmed for the wild type and E253A mutant by ESI-MS (data not shown). These data show that self-association occurs in a Ca^{2+}-independent manner.

The elution profile of OsRbohB-(138–313) after loading at a concentration of 1 mM onto a gel-filtration column showed a single but asymmetric peak, implying that the monomeric form was contaminated (Fig. 3*B*). In fact, a concentration dependence of dimer formation was observed as the protein was eluted as a monomer at a low concentration (40 μM). These data suggest that OsRbohB-(138–313) exists in a dynamic equilibrium between homodimers and monomers, and that the homodimer predominates at higher protein concentrations.

The OsRbohB-(138–313)·OsRac1 complex was eluted from a gel filtration column at a position distinct from that of the OsRbohB-(138–313) dimer. A 25:1 mixture of OsRbohB-(138–313) and OsRac1 (1 mM:40 μM) yielded a peak corresponding to the complex (Fig. 5*A*). However, a 1:25 mixture (40 μM:1 mM) did not show the complex peak (Fig. 5*B*), probably because OsRbohB-(138–313) did not form dimers. Likewise, a 1:1 mixture (40 μM:40 μM) at low total concentration provided no evidence for complex formation (Fig. 5*C*). These data strongly suggested that OsRbohB dimers are the functional units for Rac binding. Moreover, a 1:1 mixture at high total concentration (1 mM:1 mM) gave a large peak corresponding to the complex and also contained a peak representing unbound OsRac1 (Fig. 5*D*). This residual peak can be explained by assuming that OsRbohB binds to OsRac1 in a molar ratio of 2:1.

The OsRbohB-OsRac1 interaction was further analyzed by ESI-MS measurements. Peaks of 2:1 and 2:2 OsRbohB-(138–313)·OsRac1 complexes were observed in the mass spectra in addition to the equimolar, free OsRbohB-(138–313) and OsRac1 species. OsRbohB-(138–313)·OsRac1 complexes may partly dissociate during ESI-MS analysis because of instability in the gas phase. ESI-MS shows that the OsRbohB-(138–313) homodimer binds to one or two molecules of OsRac1, but does not support an unambiguous stoichiometry.

The Complete N Terminus Is Required for Binding to the C Terminus—In the case of Nox5, which possesses four EF-hand motifs in the N-terminal region, binding of Ca^{2+} to EF-hands causes a conformational change and leads to intramolecular interaction of the EF-hand domain with the C-terminal domain, resulting in Nox5 activation (32). Therefore, we investigated whether the N-terminal region binds to the C-terminal domain in OsRbohB. Surprisingly, pulldown assays using OsRbohB-(138–313) showed a very faint band (Fig. 6*B*), suggesting the EF-hand domain has a very weak affinity for the C-terminal region. When using OsRbohB-(1–137), the bound protein was somewhat more abundant, but the affinity between OsRbohB-(1–137) and C terminus still appeared weak. In contrast, OsRbohB-(1–355) including the complete N-terminal cytoplasmic region exhibited a strong affinity for the C-terminal region (Fig. 6*B*). OsRbohB-(1–306) showed a similar affinity as OsRbohB-(1–355), suggesting that residues 307–355 were not involved in the interaction. Unexpectedly, Ca^{2+} seemed to have little effect on the interaction (Fig. 6*C*). We also checked whether OsRbohB-(1–355) had a binding affinity for the cytosolic loops connecting transmembrane helices 2 and 3, and helices 4 and 5; the results were negative (Fig. 6*D*). Taken together, intramolecular interaction between with the N and C terminus occurs in Rboh as observed in Nox5, but it is Ca^{2+}-independent and requires the N-terminal region preceding the EF-hand domain in Rboh, in contrast to Nox5.

DISCUSSION

In the present study, we determined the first crystal structure of the N-terminal region that is important for regulation of

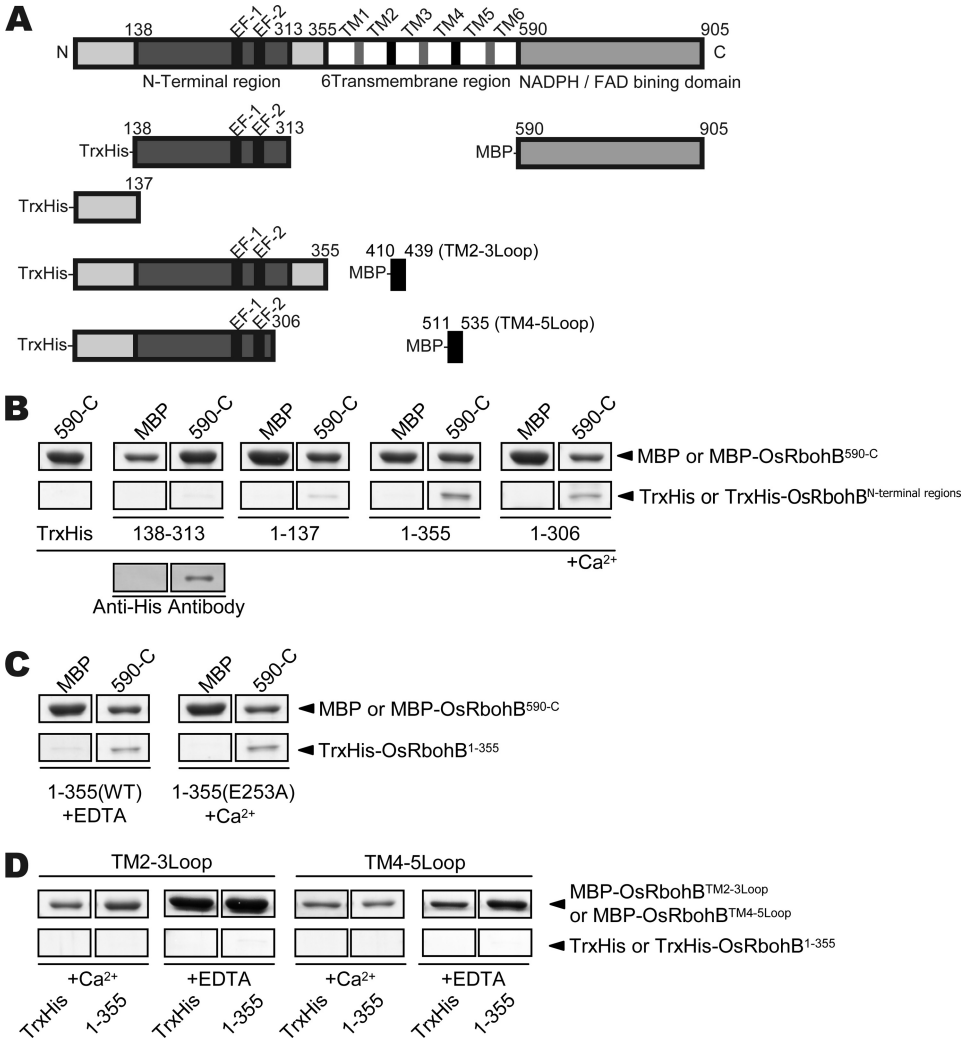

FIGURE 6. **Interaction between the N-terminal cytoplasmic region and the cytosolic C-terminal region, which carries FAD- and NADPH-binding domains.** *A*, domain structures of fragments used in pulldown assays. *B*, *in vitro* pulldown assay of MBP-OsRbohB-(590-C) with various N-terminal fragments of thioredoxin-OsRbohB (*Trx-OsRbohB*). Each N-terminal fragment of OsRbohB was incubated either with maltose binding protein (*MBP*) or with MBP-OsRbohB-(590-C). The identity of the Trx-OsRbohB-(138–313) band was confirmed by Western blotting using anti-His antibodies. *C*, effects of Ca^{2+} on the binding. EDTA-treated and E253A mutant of OsRbohB-(1–355) were incubated. No Ca^{2+} effects on the binding were observed. *D*, *in vitro* pulldown assays of MBP-OsRbohB containing a cytoplasmic loop with OsRbohB-(1–355).

Rboh. Our structural study revealed that the N-terminal cytoplasmic region contained four EF-hands (one functional EF-hand, one disabled EF-hand, and two EF-like motifs) although sequence analyses had predicted two EF-hands. EF-1 of one molecule interacts with EF-2 of another one in a domain-swapping manner to form an EF-hand domain, and vice versa. Several EF-hand proteins, such as S100 proteins, calpain, and polcalcins, naturally occur as dimers. The structural unit of S100 proteins is a symmetric dimer comprised of two EF-hand motifs, which are organized into an eight-helix bundle (33). Calpain, the penta EF-hand family, dimerizes through an interaction between their fifth EF-hand motif (EF5) (34, 35). Some polcalcins form a compact structure by domain-swapping between pairs of EF-hands (36). The dimer of RbohB exhibits an elongated shape and a coiled-coil region that forms a binding interface for Rac1. This unique structural feature is quite distinct from those in S100 proteins, calpain, or polcalcins.

The structural study also revealed that OsRbohB contains two unpredicted EF-hand-like domains, with sequences that differ markedly from those of classical EF-hands. Considering the conservation of the sequence of the N-terminal cytoplasmic region of plant NADPH oxidases (supplemental Fig. S2), they likely share a common structure featuring swapped EF-hands and unpredicted EF-hands. It is reported that enzymes of the fungal NoxC subfamily contain a single EF-hand in the N-terminal cytoplasmic region (37). Based on our results, it appears possible that NoxC might possess an EF-hand domain comprising predicted EF-hands and unpredicted EF-hands.

Rac Binding Motif—To date, a number of Rac effectors have been identified and several Rac binding motifs have been classified. The CRIB (Cdc42/Rac-interactive binding) motif consisting of about 15 residues is a common sequence motif of Rac and Cdc42 effectors. Structural studies have shown that the CRIB motif forms an intermolecular β-sheet interaction with β-strand of Rac/Cdc42 (38, 39). In addition, $p67^{phox}$, one of the subunits of phagocytic NADPH oxidases, contains tetratrico-peptide repeat domains that were identified as binding domains for Rac. The tetratrico-peptide repeat domain includes repeated α-helical motifs and β-hairpins. β-Hairpins and loops create the binding surface for Rac (40). Rac binds to the coiled-coil region of Arfaptin and the pleckstrin homology domain of phospholipase C-β2 (41). In RbohB, residues important for Rac1 binding are located in the flanking region of the coiled-coil region. This binding region is dissimilar to those previously identified as Rac binding motifs. Thus, OsRac1 interacts with OsRbohB in a manner distinct from known interactions between Rac and its target proteins.

Dimer in Solution—Our structural and physicochemical studies showed that Rboh dimerizes in a concentration-dependent by domain swapping, and that the dimers probably represent functional units. In tobacco, Rboh has been shown to be localized in lipid rafts in the plasma membrane (42), implying that the local concentrations might be high enough for dimer formation due to macromolecular crowding effects. Recently the crystal structure of Steap3 was reported (46), showing the dimerization of the $F_{420}H_2$:$NADP^+$ oxidoreductase domain. The $F_{420}H_2$:$NADP^+$ oxidoreductase domain of

Steap3 differs significantly from the ferredoxin-$NADP^+$ reductase domain, which is a C-terminal cytoplasmic domain of NADPH oxidase. The dimerization of ferredoxin-$NADP^+$ reductase in NADPH oxidases has not been reported. Rboh and Steap3 would function as a dimer, but it remains unknown whether dimerization is common for NADPH oxidases and other membrane proteins bearing the NADPH- and FAD-binding domains.

Proposed Regulation of Rboh by Ca^{2+} and Rac1—We showed that Ca^{2+} binding to the EF-hand in the N terminus of OsRbohB induced a conformational change. This Ca^{2+}-mediated change regulates Rboh activity, because Ca^{2+} binding to the EF-hands is required for ROS production by Rboh (12, 14). In fact, the E277Q mutation of AtRbohD, corresponding to the E253A mutation of OsRbohB, completely abolished ROS production (14). Similarly, the E250A mutation of RHD2, corresponding to the E253A mutation of OsRbohB, causes a 50–60% decrease in activity (12). As we demonstrated, the mutation at this position (E253A) causes no Ca^{2+}-mediated conformational change, ROS production would be expected to be abolished or decreased. Although the intramolecular interaction between the N and C terminus observed here was Ca^{2+} independent, it is evident that Ca^{2+} binding is essential for activation of OsRbohB. Probably, Ca^{2+}-mediated conformational changes lead to a precise orientation of the cytoplasmic domains that are necessary for activation through interactions of the N and C domains. It remains to be determined how phosphorylation by Ca^{2+}-dependent protein kinases as reported from potato (13) affects the regulatory mechanism in rice.

Rac1 is a component of the NADPH oxidase complex together with RACK1, RAR1, SGT1, HSP90, and HSP70 (43, 44). The precise architecture of this Rac1 immune complex probably plays a crucial role in the production of ROS (supplemental Fig. S3). Further studies will reveal whether Ca^{2+}-mediated conformational changes in Rboh contribute to Rac1 immune complex formation.

Acknowledgments—We thank the staffs of SPring-8 and PF for data collection.

REFERENCES

1. Doke, N. (1983) *Phyisol. Plant Pathol.* **23,** 345–357
2. Groom, Q. J., Torres, M. A., Fordham-Skelton, A. P., Hammond-Kosack, K. E., Robinson, N. J., and Jones, J. D. (1996) *Plant J.* **10,** 515–522
3. Keller, T., Damude, H. G., Werner, D., Doerner, P., Dixon, R. A., and Lamb, C. (1998) *Plant Cell* **10,** 255–266
4. Torres, M. A., Onouchi, H., Hamada, S., Machida, C., Hammond-Kosack, K. E., and Jones, J. D. (1998) *Plant J.* **14,** 365–370
5. Yoshioka, H., Sugie, K., Park, H. J., Maeda, H., Tsuda, N., Kawakita, K., and Doke, N. (2001) *Mol. Plant Microbe Interact.* **14,** 725–736
6. Yoshioka, H., Numata, N., Nakajima, K., Katou, S., Kawakita, K., Rowland, O., Jones, J. D., and Doke, N. (2003) *Plant Cell* **15,** 706–718
7. Sagi, M., and Fluhr, R. (2006) *Plant Physiol.* **141,** 336–340
8. Torres, M. A., and Dangl, J. L. (2005) *Curr. Opin. Plant Biol.* **8,** 397–403
9. Bánfi, B., Molnár, G., Maturana, A., Steger, K., Hegedûs, B., Demaurex, N., and Krause, K. H. (2001) *J. Biol. Chem.* **276,** 37594–37601
10. Edens, W. A., Sharling, L., Cheng, G., Shapira, R., Kinkade, J. M., Lee, T., Edens, H. A., Tang, X., Sullards, C., Flaherty, D. B., Benian, G. M., and Lambeth, J. D. (2001) *J. Cell Biol.* **154,** 879–891
11. Sagi, M., and Fluhr, R. (2001) *Plant Physiol.* **126,** 1281–1290
12. Takeda, S., Gapper, C., Kaya, H., Bell, E., Kuchitsu, K., and Dolan, L. (2008) *Science* **319,** 1241–1244
13. Kobayashi, M., Ohura, I., Kawakita, K., Yokota, N., Fujiwara, M., Shimamoto, K., Doke, N., and Yoshioka, H. (2007) *Plant Cell* **19,** 1065–1080
14. Ogasawara, Y., Kaya, H., Hiraoka, G., Yumoto, F., Kimura, S., Kadota, Y., Hishinuma, H., Senzaki, E., Yamagoe, S., Nagata, K., Nara, M., Suzuki, K., Tanokura, M., and Kuchitsu, K. (2008) *J. Biol. Chem.* **283,** 8885–8892
15. Kawasaki, T., Henmi, K., Ono, E., Hatakeyama, S., Iwano, M., Satoh, H., and Shimamoto, K. (1999) *Proc. Natl. Acad. Sci. U.S.A.* **96,** 10922–10926
16. Ono, E., Wong, H. L., Kawasaki, T., Hasegawa, M., Kodama, O., and Shimamoto, K. (2001) *Proc. Natl. Acad. Sci. U.S.A.* **98,** 759–764
17. Wong, H. L., Pinontoan, R., Hayashi, K., Tabata, R., Yaeno, T., Hasegawa, K., Kojima, C., Yoshioka, H., Iba, K., Kawasaki, T., and Shimamoto, K. (2007) *Plant Cell* **19,** 4022–4034
18. Kawasaki, T., Koita, H., Nakatsubo, T., Hasegawa, K., Wakabayashi, K., Takahashi, H., Umemura, K., Umezawa, T., and Shimamoto, K. (2006) *Proc. Natl. Acad. Sci. U.S.A.* **103,** 230–235
19. Oda, T., Hashimoto, H., Kuwabara, N., Hayashi, K., Kojima, C., Kawasaki, T., Shimamoto, K., Sato, M., and Shimizu, T. (2008) *Acta Crystallogr. Sect. F Struct. Biol. Cryst.* **64,** 867–869
20. Otwinowski, Z., and Minor, W. (1997) *Methods Enzymol.* **276,** 307–326
21. Terwilliger, T. C., and Berendzen, J. (1999) *Acta Crystallogr. Sect. D Biol. Crystallogr.* **55,** 849–861
22. Terwilliger, T. C. (2000) *Acta Crystallogr. Sect. D Biol. Crystallogr.* **56,** 965–972
23. Perrakis, A., Sixma, T. K., Wilson K. S., and Lamzin, V. S. (1997) *Acta Crystallogr. Sect. D Biol. Crystallogr.* **53,** 448–455
24. Emsley, P., and Cowtan, K. (2004) *Acta Crystallogr. Sect. D Biol. Crystallogr.* **60,** 2126–2132
25. Brünger, A. T., Adams, P. D., Clore, G. M., DeLano, W. L., Gros, P., Grosse-Kunstleve, R. W., Jiang, J. S., Kuszewski, J., Nilges, M., Pannu, N. S., Read, R. J., Rice, L. M., Simonson, T., and Warren, G. L. (1998). *Acta Crystallogr. Sect. D Biol. Crystallogr.* **54,** 905–921
26. Murshudov, G. N., Vagin, A. A., and Dodson, E. J. (1997) *Acta Crystallogr. Sect. D Biol. Crystallogr.* **53,** 240–255
27. Laskowski, R. A., MacArthur, M. W., Moss, D. S., and Thornton, J. M. (1993) *J. Appl. Crystallogr.* **26,** 283–291
28. Delano, W. L. (2002) *The PyMOL Molecular Graphics System,* Delano Scientific, San Carlos, CA
29. Reynolds, C., Damerell, D., and Jones, S. (2009) *Bioinformatics* **25,** 413–414
30. Holm, L., and Sander, C. (1995) *Trends Biochem. Sci.* **20,** 478–480
31. Collaborative Computational Project 4 (1994) *Acta Crystallogr. Sect. D Biol. Crystallogr.* **50,** 760–763
32. Bánfi, B., Tirone, F., Durussel, I., Knisz, J., Moskwa, P., Molnár, G. Z., Krause, K. H., and Cox, J. A. (2004) *J. Biol. Chem.* **279,** 18583–18591
33. Potts, B. C., Smith, J., Akke, M., Macke, T. J., Okazaki, K., Hidaka, H., Case, D. A., and Chazin, W. J. (1995) *Nat. Struct. Biol.* **2,** 790–796
34. Blanchard, H., Grochulski, P., Li, Y., Arthur, J. S., Davies, P. L., Elce, J. S., and Cygler, M. (1997) *Nat. Struct. Biol.* **4,** 532–538
35. Lin, G. D., Chattopadhyay, D., Maki, M., Wang, K. K., Carson, M., Jin, L., Yuen, P. W., Takano, E., Hatanaka, M., DeLucas, L. J., and Narayana, S. V. (1997) *Nat. Struct. Biol.* **4,** 538–547
36. Verdino, P., Westritschnig, K., Valenta, R., and Keller, W. (2002) *EMBO J.* **21,** 5007–5016
37. Aguirre, J., Ríos-Momberg, M., Hewitt, D., and Hansberg, W. (2005) *Trends Microbiol.* **13,** 111–118
38. Mott, H. R., Owen, D., Nietlispach, D., Lowe, P. N., Manser, E., Lim, L., and Laue, E. D. (1999) *Nature* **399,** 384–388
39. Abdul-Manan, N., Aghazadeh, B., Liu, G. A., Majumdar, A., Ouerfelli, O., Siminovitch, K. A., and Rosen, M. K. (1999) *Nature* **399,** 379–383
40. Lapouge, K., Smith, S. J., Walker, P. A., Gamblin, S. J., Smerdon, S. J., and Rittinger, K. (2000) *Mol. Cell* **6,** 899–907
41. Jezyk, M. R., Snyder, J. T., Gershberg, S., Worthylake, D. K., Harden, T. K., and Sondek, J. (2006) *Nat. Struct. Mol. Biol.* **13,** 1135–1140
42. Mongrand, S., Morel, J., Laroche, J., Claverol, S., Carde, J. P., Hartmann, M. A., Bonneu, M., Simon-Plas, F., Lessire, R., and Bessoule, J. J. (2004)

J. Biol. Chem. **279,** 36277–36286
43. Thao, N. P., Chen, L., Nakashima, A., Hara, S., Umemura, K., Takahashi, A., Shirasu, K., Kawasaki, T., and Shimamoto, K. (2007) *Plant Cell* **19,** 4035–4045
44. Nakashima, A., Chen, L., Thao, N. P., Fujiwara, M., Wong, H. L., Kuwano, M., Umemura, K., Shirasu, K., Kawasaki, T., and Shimamoto, K. (2008) *Plant Cell* **20,** 2265–2279
45. Davis, I. W., Leaver-Fay, A., Chen, V. B., Block, J. N., Kapral, G. J., Wang, X., Murray, L. W., Arendall, W. B., 3rd, Snoeyink, J., Richardson, J. S., and Richardson, D. C. (2007) *Nucleic Acids Res.* **35,** W375–W383
46. Sendamarai, A. K., Ohgami, R. S., Fleming, M. D., and Lawrence, C. M. (2008) *Proc. Natl. Acad. Sci. U.S.A.* **105,** 7410–7415